TITLE PAGE

Title: Seismic and Rockphysics Diagnostics of Multiscale Reservoir Textures

Type of Report: Quarterly Technical

Reporting Start Date: April 1, 2004

Reporting End Date: June 30, 2004

Principal Investigator: Prof. Gary Mavko

Date of Report: August 2004

DOE Award Number: DE-FC26-01BC15354

Submitting Organization: Stanford University, 651 Serra Street, Suite 260, Stanford, CA 94305-4125

DISCLAIMER

ABSTRACT

As part of our study on “Relationships between seismic properties and rock microstructure”, we have continued our work on analyzing well logs and microstructural constraints on seismic signatures. We report results of three studies in this report. The first one deals with fractures and faults that provide the primary control on the underground fluid flow through low permeability massive carbonate rocks. Fault cores often represent lower transmissibility whereas the surrounding damaged rocks and main slip surfaces are high transmissibility elements. We determined the physical properties of fault rocks collected in and around the fault cores of large normal faults in central Italy. After studying the P- and S-wave velocity variation during cycles of confining pressure, we conclude that a rigid pore frame characterizes the fault gouge whereas the fractured limestone comprises pores with a larger aspect ratio. The second study was to characterize the seismic properties of brine as its temperature decreases from 25 ºC to –21ºC. The purpose was to understand how the transmitted wave changes with the onset of freezing. The main practical reason for this experiment was to use partially frozen brine as an analogue for a mixture of methane hydrate and water present in the pore space of a gas hydrate reservoir. In the third study we analyzed variations in dynamic moduli in various carbonate reservoirs. The investigations include log and laboratory data from velocity, porosity, permeability, and attenuation measurements.

TABLE OF CONTENTS

LIST OF GRAPHICAL MATERIALS

DOE F 4600.6
(10-94)
Replaces EIA-459F
All Other Editions Are Obsolete

U.S. DEPARTMENT OF ENERGY
FEDERAL ASSISTANCE PROGRAM/PROJECT STATUS REPORT

OMB Control No.
1910-0400

OMB Burden Disclosure Statement

Public reporting burden for this collection of information is estimated to average 47.5 hours per response, including the time for reviewing instructions, searching existing data sources, gathering and maintaining the data needed, and completing and reviewing the collection of information. Send comments regarding this burden estimate or any other aspect of this collection of information, including suggestions for reducing this burden, to Office of Information Resources Management Policy, Plans, and Oversight, Records Management Division, HR-422 - GTN, Paperwork Reduction Project (1910-0400), U.S. Department of Energy, 1000 Independence Avenue, S.W., Washington, DC 20585; and to the Office of Management and Budget (OMB), Paperwork Reduction Project (1910-0400), Washington, DC 20503.

1. Program/Project Identification No. **DE-FC26-01BC15354**	2. Program/Project Title **Seismic and Rock-Physics Diagnostics of Multiscale Reservoir Textures**	3. Reporting Period **4/1/04** through **6/30/04**
4. Name and Address **Professor Gary Mavko (Research)** **Geophysics Department,** **Stanford University, 397 Panama Mall, Stanford, CA 94305-2215**		5. Program/Project Start Date **9/17/2001** 6. Completion Date **9/16/2004**

7. Approach Changes

☒ None

8. Performance Variances, Accomplishments, or Problems

☐ None

9. Open Items

☒ None

10. Status Assessment and Forecast

☒ No Deviation from Plan is Expected

11. Description of Attachments

☒ None

12. Signature of Recipient and Date	13. Signature of U.S. Department of Energy (DOE) Reviewing Representative and Date

No further monies or other benefits may be paid out under this program unless this report is completed and filed as required by existing law and regulations (DOE Organizational Act; PL 95-91 42 USC 7254 and Federal Grant and Cooperative Agreement Act of 1977 PL 95-224 (41 USC 508).

FEDERAL ASSISTANCE PROGRAM/PROJECT STATUS REPORT

PURPOSE

A concise narrative describing the current status of the effort. The report allows Federal assistance recipients to communicate developments, achievements, changes and problems to the U.S. Department of Energy (DOE).

INSTRUCTIONS

Item 1 - Enter the Federal grant or agreement identification number for the current year as it appears in the official award.

Item 2 - Enter the program/project official title as it appears in the award and, if applicable, the project identification number.

Item 3 - Enter the start and completion dates for the current reporting period.

Item 4 - Enter the name and address of the recipient office responsible for managing the project.

Item 5 - Enter the official start date of the original agreement.

Item 6 - Enter the official completion date as of the latest modification.

Item 7 - Provide a description of any changes from the work plan, including technical changes, the explanation as to why these changes occurred, and what the impact on performance will be. If there were no changes during the reporting period, check the box for "none."

Item 8 - Include a discussion of accomplishments, problems and/or variances, their causes and the effects on the effort. If no performance variances, accomplishments, nor problems occurred during the reporting period, check "none."

Item 9 - Discuss any unresolved issues or items that require action by DOE or recipient. If there are no unresolved issues which require action or coordination, check "none."

Item 10 - Present analysis of program/project status, proposed solutions to problems, and future expectations regarding the project. If no deviations from the plan are forecast, enter a check in the box provided.

Item 11 - Provide a short list of program/project related attachments. If no attachments accompany the report, check "none."

Item 12 - The recipient should sign and date the report so that, if questions arise, they can be directed to the appropriate individual.

Item 13 - The DOE reviewing representative, usually the DOE program manager responsible for monitoring the program, signs and dates the form to indicate it has been reviewed and appears reasonable.

DOE F 4600.3A
(09-92)

OMB Control No.
1910-0400

U.S. Department of Energy
Milestone Log

OMB Burden Disclosure Statement

Seismic and Rock-Physics Diagnostics of Multiscale Reservoir Textures

Program/Project Title

Identification Number	Description	Planned Completion Date	Actual Completion Date	Comments
I.1	Acoustic Microscopy	5/31/03	5/31/03	COMPLETED
1.2	Compare With laboratory wave propagation	11/30/02	11/30/02	COMPLETED
I.3	Theoretical Analysis	8/31/04		ONGOING
I.4	Scale Seismic properties & Texture	8/31/04		ONGOING
II.1	Experiments	8/31/02	8/31/02	COMPLETED
II.2	Theoretical Analysis	8/31/04		ONGOING
II.3	Upscale Attributes	8/31/04		ONGOING
III.1	Velocity Upscaling	2/29/04	2/29/04	COMPLETED
III.2	Multi-Scale Transforms	8/31/04		ONGOING

INTRODUCTION

In this quarter, we submit results of our work on analyzing well log response in chalks and on the correlations between transport and seismic properties in carbonate rocks. We also present some results of an experimental study on the elastic and anelastic properties of brines and brine-ice. The carbonate rocks paper deals with fractures and faults that provide the primary control on the underground fluid flow through low permeability massive carbonate rocks. Fault cores often represent lower transmissibility whereas the surrounding damaged rocks and main slip surfaces are high transmissibility elements. We determined the physical properties of fault rocks collected in and around the fault cores of large normal faults in central Italy. After studying the P- and S-wave velocity variation during cycles of confining pressure, we conclude that a rigid pore frame characterizes the fault gouge whereas the fractured limestone comprises pores with a larger aspect ratio. The experimental study was to characterize the seismic properties of brine as its temperature decreases from 25 ºC to – 21ºC. The purpose was to understand how the transmitted wave changes with the onset of freezing. The main practical reason for this experiment was to use partially frozen brine as an analogue for a mixture of methane hydrate and water present in the pore space of a gas hydrate reservoir. In our analyses of well log response in chalks, we have investigated variations in dynamic moduli in various carbonate reservoirs. The investigations include log and laboratory data from velocity, porosity, permeability, and attenuation measurements.

PAPER 1

Agosta, Prasad, and Aydin: ROCK PHYSICAL PROPERTIES OF CARBONATE FAULT ROCKS, FUCINO BASIN (CENTRAL ITALY)

Paper 1: Total of four figures in paper

Rock Physical properties of carbonate fault rocks, Fucino basin (central Italy)

[1]Fabrizio Agosta, [2]Manika Prasad, and [1]Atilla Aydin, [1]Department of Geological and Environmental Sciences and [2]Department of Geophysics, Stanford University, CA.*

Summary

Fractures and faults provide the primary control on the underground fluid flow through low permeability massive carbonate rocks. Fault cores often represent lower transmissibility whereas the surrounding damaged rocks and main slip surfaces are high transmissibility elements. We determined the physical properties of fault rocks collected in and around the fault cores of large normal faults in central Italy. The cemented fault rocks present along the main slip surfaces have low porosity and high bulk and shear moduli, which are very similar to those characterizing the Cretaceous limestone host rock. Conversely, the fault gouge within the fault cores and the fractured limestone have higher low porosity and high bulk and shear moduli relative to the host rock. These two rocks are however composed by a different pore frame. After studying the P- and S-wave velocity variation during cycles of confining pressure, we conclude that a rigid pore frame characterizes the fault gouge whereas the fractured limestone comprises pores with a larger aspect ratio.

Introduction

Both geometrical and physical properties of faults and fault rocks are the main parameters used to evaluate how faults impact the subsurface fluid flow. In general, the geometrical arrangement of fault-related structures is tied together with porosity and permeability measurements performed on fault rock samples to calculate fault transmissibility (Walsh et al., 1998; Manzocchi et al., 1999) and upscaled fault permeability (Flodin, 2003). The goal of this study is to determine the physical properties of both host and fault rocks. In particular, we study the pore geometry of the different fault rocks collected in and around the fault core of the strands of large normal faults in order to understand the microstructure of the fault rock and its relation to fluid flow.

The study samples have been collected along and across the normal faults bounding the eastern side of the Fucino basin, central Italy. The faults strike N110-140, dip 50° to 65°, and form a SW-dipping fault zone. The fault zone bordering the basin accommodated as much as 0.8 km of offset, which rapidly decreases towards zero at the fault tips. Their internal structure consists of brecciated Quaternary sediments in the hanging wall, and meter(s) thick fault core of cemented and matrix-supported fault rock (fault gouge) and breccia in the footwalls. The faults are surrounded by less-damaged fractured carbonates, which are up to ten(s) of meter thick. The primary mechanism of deformation of these rocks is the sequential formation and shearing of solution seams along sheared fractures (Graham et al., 2003). The cm-wide zones of cemented fault rocks localized along the main slip surfaces in the adjacent granular fault rock. The cements are composed of low-Mg calcite, and precipitated from original meteoric fluids that mixed with the local groundwater and/or soil before entering the faults (Agosta and Kirschner, 2003).

Experimental Procedure

Two hand samples of the Upper Cretaceous limestone host rock, the *Calcare Massiccio* formation, and seven samples of fault rocks have been thin-sectioned for mineralogic analysis. Each sample was cut along the two directions orthogonal to the bedding/fault surface. A total of 16 thin-sections, two for each of the eight rock samples, have been studied under the optical microscope by using cross-polarized, transmitted light. The focus of this study is the mineral characterization of all diagenetic phases present within the host rock, and the structural characterization of abutting and crosscutting relations among the fractures present in the fault rocks. Results of XRF analyses of sample powders obtained by cemented specimens collected in the same area are also reported in Table 1.

Porosity and ultrasonic measurements were conducted on cylindrical core samples with 25 mm diameter and 20-30 mm length, which were prepared with their faces parallel to within 100 μm (Table 2). One sample was prepared from each hand specimen collected in the field. The axis of these cylindrical samples is orthogonal to the faults' strike. The axis of the sample drilled from the limestone host specimen is parallel to the bedding. Bulk and grain densities and porosity were measured using a Helium porosimeter. The pulse transmission technique was used for P- and S-wave velocity (V_P, V_S, respectively) measurements. Experiments were conducted during cycles of confining pressure, Pc (cf., Prasad et al., 1999, 2003; Vanorio et al., 2003).

Ca (wt %)	Mg (wt %)	Fe (wt %)	Sr (ppm)	Si (wt %)
39.2	0.37	0.02	162	0.07
39.2	0.35	0.06	178	0.29
32.8	4.23	0.16	36	0.83
33.2	4.72	0.05	87	0.15
28.7	7.4	0.23	52	0.44
39.4	0.2	0.04	77	0.17
26.6	8.67	0.1	55	0.35
39.1	0.17	0.03	70	0.13
34.3	3.22	0.1	45	0.13
39.5	0.11	b.d.	26	0.03
25.8	9.66	0.01	56	0.06

Table 1: Results of XRF analysis of powder samples obtained from host rock (red) and cemented fault rocks (black) collected along

large normal faults in central Italy (data from Agosta and Kirschner, 2003).

ϕ	ρs	ρb
0.8	2.73	2.706
0.56	2.705	2.681
0.6	2.713	2.697
1.27	2.721	2.686
1.6	2.68	2.635
1.3	2.635	2.601
3	2.709	2.584
5.2	2.696	2.555
2.5	2.667	2.602

Table 2: Main petrophysical properties of the nine rock samples object of this study. Porosity, grain and bulk density are shown in this table. Both host rock and cemented fault rocks values are shown in red. Values of fractured host rock and fault rock are in black.

Results of Mineralogical analysis

Mineralogical analysis of the samples shows that the limestone host rock is composed of platform-related boundstones with dark and very-small lime mud filling the pore-space (Figure 1A). The platform carbonate rocks formed in the Upper Cretaceous and underwent two main diagenetic phase: the early marine and the late burial diagenesis. Soon after deposition, micritic crusts formed around and enveloped the fossils. These crusts provided the substrate on which acicular cement (originally aragonite, now calcite) and ulterior micritic crusts precipitated. Marine diagenesis also involved in the re-crystallization of lamellar calcite within fossils and formation of lime-mud from the original calcareous algae present in the rock. Sparry calcite precipitated within the pores during the later phase of burial diagenesis. Since the sparse presence of this calcite in the thin-sections and the lack of evidences for strong compaction, this boundstone rock was characterized by very-low porosity at the moment of burial diagenesis.

The fault rock formed due to dissolution of the host rock along localized zones of deformations, in the form of solution seams, and their subsequent shearing. A few meters wide belts adjacent to, and on either sides of the fault cores of large faults, the original lithology of the host rock is still discernable. Fractures crosscut the limestone and form localized zones of enhanced deformation along minor fault with m-slip. Within the fault core, comminution and fragmentation of the fractured host rocks occur at microscale due to cataclastic deformation. The effect of this process is the formation of matrix-supported fault rocks, which are often bounded by major slip surfaces. These rocks are composed of angular-to-subrounded survivor clasts embedded in fine calcite matrix (Figure 1B). The texture of a tiny cataclastic band within the matrix-supported gouge is shown in this photograph. Occasionally, low-Mg calcite cement is present in the fault rock either within fractures or as meniscus cement.

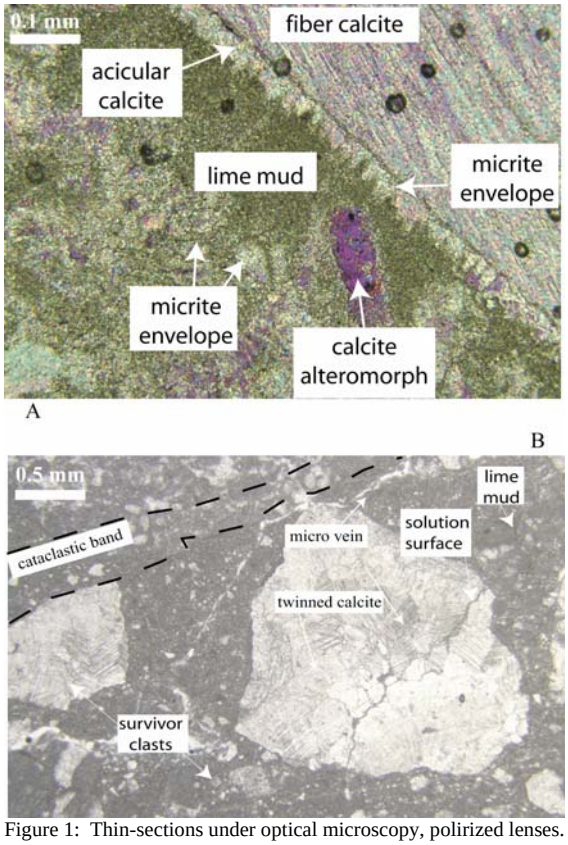

Figure 1: Thin-sections under optical microscopy, polirized lenses. A: Upper Cretaceous limestone host rock, *Calcare Massiccio* formation. B: Fault gouge rock collected in the footall of the *Venere-Gioia dei Marsi* normal fault, 0.5 m away from the main slip surface.

Results of Porosity and Ultrasonic analyses

We present here results of analyses performed on intact and fractured limestone host rocks, and cemented and not-cemented fault gouge. The legend for the plots of ultrasonic velocity measurements is shown on Figure 2. Figure 3A and B report the results of our P- and S-wave velocity measurements during cycles of confining pressure. High P-wave velocity characterizes the two cemented fault rock samples. Their velocity increases slightly during the first increments of Pc, and then it forms plateau around 5.8 km/sec. This behaviour is similar to the host rock P-wave velocity trend, which increases slightly only during the first steps of Pc and then remains stable at values ~5.65 km/sec. All the three aforementioned samples, cemented fault rock

and limestone host rock, are characterized by a small hysteresis during cycles of Pc. Conversely, both the fractured limestone and fault gouge show a significant hysteresis and lower values of P-wave velocity. In particular, Vp increases significantly in the four fractured samples during the first increments of Pc and then it stabilized around values of 5.4-5.5 km/sec. In contrast, the fault gouge has lower Vp, which can be as low as ~5.2 km/sec, and it changes a more uniformly during all the increments of Pc.

Vs shows a similar behaviour as Vp. Both cemented fault rocks and limestone host rock have high S-wave velocity, which plateaus at around 3.15 km/sec under increasing Pc. These values are a little higher of those of the fractured limestone, which can range between 3.05 and 3.1 km/sec. The S-wave velocity of these fractured samples increases significantly during the first increments of Pc, which is not shown for the other study samples. S-wave velocity values of 2.9-3.0 km/sec characterize the fault gouge.

Figures 3C and D represent that variation of the elastic moduli during cycles of pressure. The cemented fault rocks have values of K of ~ 55 GPa, the limestone host rock of ~ 49 Gpa. These two values are higher that those of fractured limestone, which ranges between 34 and 44 Gpa, and fault gouge. The shear modulus of both host and cemented rocks is ~ 27Gpa, and it does not change significantly during increasing confining pressure. The fault gouge has the lowest values of μ among the study samples.

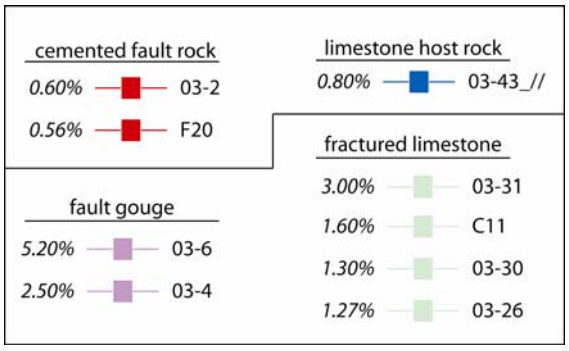

Figure 2: Legend of the following plots of ultrasoinc velocity measurements. Four main groups of samples have been analyzed: both cemented fault rock and host rock have similar physical properties. The number on the left of the symbol represents the porosity at Pc=0.

We now examine the affect of porosity on the elastic properties of the study samples (Figure 4). Results The k-ϕ (Figure 4A) and μ-ϕ (4B) plots are consistent with the increase of the elastic moduli and decrease of porosity as Pc increases. This behaviour is more pronounced in the fractured limestone samples, whereas it is less marked in the fault gouge. Both host rock and cemented fault rocks do not show significant changes of k and μ with lower porosity.

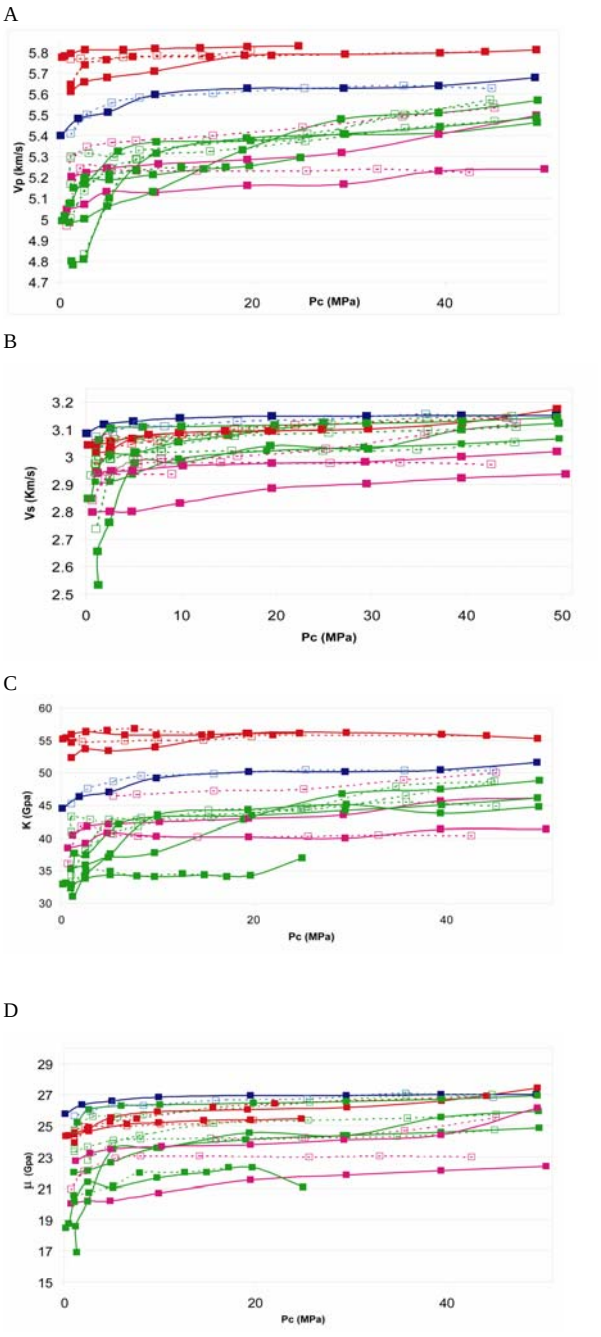

Figure 3: Results of ultrasonic experiments performed under cycles of confining pressure. A: P-wave velocity; B: S-wave velocity; C: bulk modulus, K; D:shear modulus, μ.

A

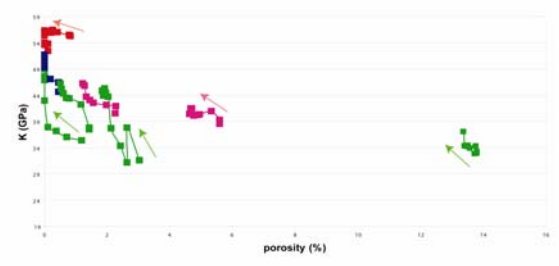

B

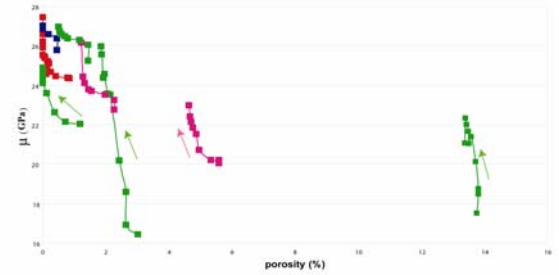

Figure 4: Variation of elastic moduli k and μ relative to changes in ϕ during increment of Pc. The arrows in the plots represents direction of increasing pressure during the experiments. A: bulk modulus, K; B:shear modulus, μ.

Conclusions

Our results of porosity and ultrasonic experiments show that both host and cemented fault rock samples have low ϕ, high Vp, Vs, K, and μ relative to the fractured and fault gouge samples. The pressure dependence of P- and S-wave velocities in the fractured samples vary according to their original porosity: samples with higher original porosity show a sharper increase of Vp and Vs under increasing confining pressure (Pc). These velocity changes during cycles of Pc show that pores in the fractured host rocks are soft and with large aspect ratio, which is consistent with the presence of the presence of crack-like pores in the rock. Conversely, the fault gouge samples are characterized by high porosity. The P- and S-wave velocity show a short increase under increasing Pc forming then plateaus, which represents the occurrence of a hard pore frame –no fractures- in the rock. The whole rock is thus characterized by sub-spherical pores that localize within the lime mud, and by solution seams that are less pervasive relative to the fractured limestone.

Both the presence of localized carbonate cements in the fault zones, and the very low permeability of both fault rocks and damaged host rocks indicate that the study faults act as both conduits and barriers. Due to the low values of permeability, faults are effective barriers to cross flow and, provide conduits only for fault-parallel flow via high permeability slip surfaces. These surfaces are present both at the hanging wall-footwall contact and within the damage zones. This permeability structure thus determines the fluid compartmentalization in and around the main slip surfaces.

References

Agosta, F., and D.L. Kirschner, 2003, Fluid conduits in carbonate-hosted seismogenic normal faults of Central Italy, Journal of Geophysical Research, 108, B4, 2221, doi: 101029/2002JB002013.

Flodin, E.A., 2003, Structural evolution, petrophysics, and large-scale permeability of faults in sandstone, Valley of Fire, Nevada, Ph.D. Thesis, Stanford University (CA), p. 180.

Graham, B. M. Antonellini, and A. Aydin, 2003, Formation and growth of normal faults in carbonates within a compressive environment, Geology, 31, 11-14.

Klinkby, L., 2001, Geophysical logging and hydraulic testing in a fractured carbonate, Abstracts with Programs – Geological Society of America, 33, 168.

Manzocchi, T., J.J. Walsh, P. Nell, and G. Yielding, 1999, Fault transmissibility multipliers for flow simulation models, Petroleum Geoscience, 5, 53-63.

Prasad, M., Nur, A., 2003, Velocity and attenuation anisotropy in reservoir rocks, Expanded Abstracts of 2003 SEG Annual Meeting, Paper RP 2.3.

Prasad, M., Palafox, G. & Nur, A., 1999. Velocity and Attenuation Characteristics of Daqing sandstones: Effects of permeability on velocity and attenuation anisotropy, AGU 1999 Fall Meeting, EOS Transaction American Geophysical Union, v, 80.

Vanorio, T., Prasad, M., Nur, A., Patella, D., 2002, Ultrasonic velocity measurements in volcanic rocks: correlation with microtexture, Geophysical Journal International, v. 149, #1, 22 - 36.

Walsh, J.J., J. Watterson, A.E. Heath, and C. Childs, 1998, Representation and scaling of faults in fluid flow models, Petroleum Geoscience, 4, 241-251.

Acknowledgements

We acknowledge support from the Rock Fracture Project (RFP) and Rock Physics and Borehole (SRB) projects at Stanford University, and thank Jonathan Stebbins and Karlheinz Merkle for providing us access to their labs. We also acknowledge support from the DOE (Award No. DE-FC26-01BC15354). Part of FA's fieldwork in central Italy has been supported by a Stanford McGee grant.

PAPER 2

Prasad and Dvorkin: VELOCITY AND ATTENUATION OF COMPRESSIONAL WAVES IN BRINES

Paper 1: Total of six figures in paper

Velocity and Attenuation of Compressional Waves in Brines

Manika Prasad and Jack Dvorkin, Stanford University and Rock Solid Images*

Summary

We conducted an acoustic pulse transmission experiment in brine as its temperature decreased from 25 ºC to – 21ºC. The purpose was to understand how the transmitted wave changes with the onset of freezing. The main practical reason for this experiment was to use partially frozen brine as an analogue for a mixture of methane hydrate and water present in the pore space of a gas hydrate reservoir. The results indicate that as the brine cools, the P-wave velocity decreases from 1500 m/s to 1480 m/s. With the onset of freezing, the velocity begins to increase until it reaches a maximum of 3700 m/s. Counter to our intuition, this increase in the velocity is accompanied by a strong reduction of the signal's amplitude and frequency content. The signal quality does not recover even after a brine sample was kept frozen at – 21ºC for over two months. This result may partly explain the reported effect that the attenuation in methane hydrate sediment is relatively large although the hydrate in the pore space acts to dramatically increase the velocity.

Introduction

Brine reacts to freezing very differently than pure water. While the latter becomes solid ice as the temperature falls below freezing, the former remains slush even at very low temperatures. The reason for this behavior is that salty water does not freeze and the ice generated from brine is always fresh. As larger and larger portions of brine turn into fresh ice, the remaining liquid pockets become more and more concentrated which further inhibits the freezing.

We have decided to investigate the effect of this behavior on the acoustic properties. One reason was scientific curiosity – to the best of our knowledge, such experimental data are nonexistent.

The other reason was practical. Unexpectedly large attenuation in sediments with gas hydrates has been recently observed at different geographical locations, in different depositional environments, and at different frequency (Guerin et al., 1999; Sakai, 1999; Wood et al., 2000; Guerin and Goldberg, 2002; Pratt et al., 2003).

Experimenting with methane hydrate is expensive and difficult. This is why we decided to use frozen brine where ice and salty water coexist at the pore-scale level as an elastic analogy to methane hydrate and seawater present in the pore space of sediment. These experiments are not intended to entirely explain the mechanism of elastic-wave attenuation in methane hydrate reservoir but rather partially unveil it.

Experimental Setup

The experimental setup consisted of a Plexiglas container that held the brine. Immersion transducers (1 MHz Panametrics Transducers V303-SU) were positioned on two sides of the container such that their distance was fixed during the experiment (Figures 1 and 2).

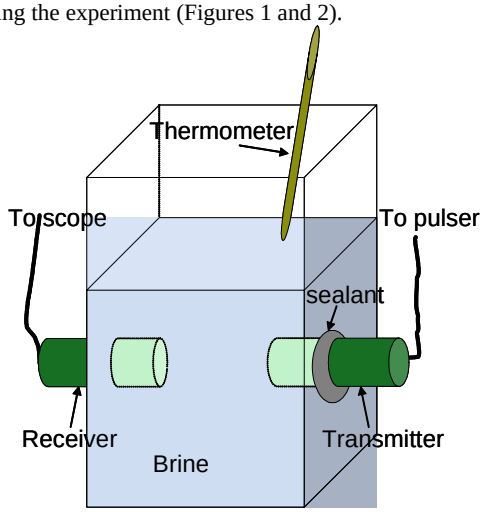

Figure 1. Experimental setup (a scheme) used in the study. The transducers are immersed in the brine at all times and freeze together with it.

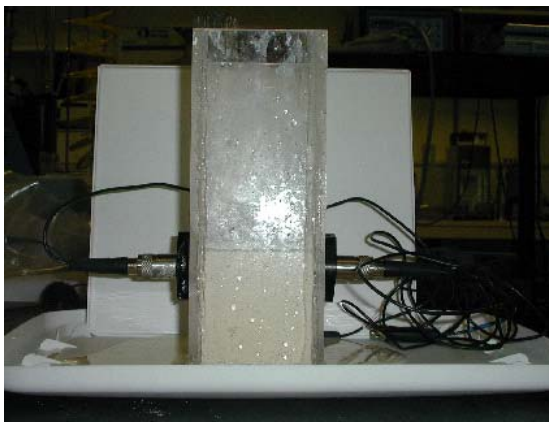

Figure 2. Experimental setup (photograph)

The transducers were excited using a Panametrics pulser. The signals through the brine were received and digitized by a Tektronix oscilloscope.

The brine was a solution of NaCl in distilled water with concentration 50,000 parts per million. It was de-aired in vacuum.

The whole setup was placed in the freezer. With the onset of freezing, the slush was mechanically stirred to ensure homogeneous distribution of ice crystals in the brine.

Results

Figure 3 shows the waveforms as the brine cools. Above freezing, the waveforms do not noticeably react to temperature variations, except for a small delay in the arrival time and reduction in the peak-to-peak amplitude as the brine becomes cooler.

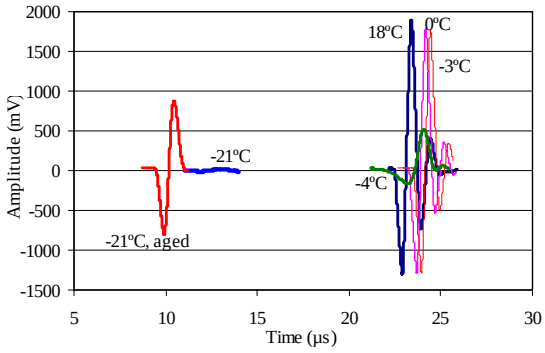

Figure 3. Waveforms registered in the cooling and freezing brine with temperature marked. There is a significant reduction in signal amplitude and frequency as the brine freezes. At -21ºC the amplitude is reduced by almost a factor of 100 (bold blue waveform on the left side of the graph), while the velocity is almost doubled. After two months in the freezer, the velocity increases slightly (red waveform on the left side of the graph). However, the amplitude does not fully recover.

However, there is a significant reduction in signal amplitude and frequency as the brine freezes. At -21ºC the signal amplitude is reduced by about two orders of magnitude, while the velocity is almost doubled.

After two months in the freezer, as the frozen brine matures, the velocity increases slightly. At the same time, the amplitude recovers but only to half of its original value at 18ºC (Figure 3 and Table 1).

Figure 4 shows normalized amplitude frequency spectra of the waveforms versus temperature. The spectra were calculated from the first cycle of the corresponding waveforms.

Above freezing, the frequency content of the waveforms does not change. However, there is a significant reduction in signal frequency as the brine freezes. At -21ºC the principal frequency of the signal is reduced to almost one-third of its original value (from about 740 kHz to 200 kHz). After two months at -21ºC, the signal recovers almost 85% of its original frequency content at 18ºC.

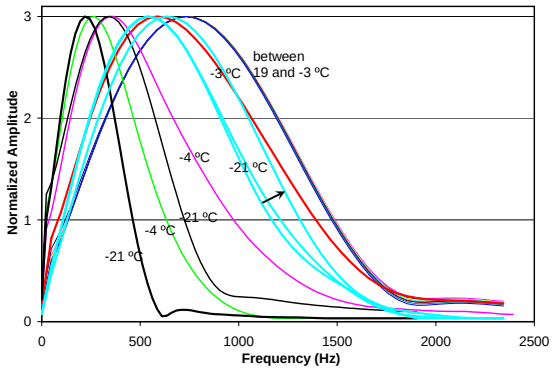

Figure 4. Normalized waveform spectra. The thick black and cyan colored lines show spectra at -21ºC. The black colored spectra was measured in the frozen brine after only a few hours. The cyan colored spectra show changes during the two months that the setup remained at -21ºC. The small arrow marks increasing time.

Table 1: Velocity, frequency, and amplitude versus temperature.

Temperature (ºC)	Velocity (m/s)	Principal Frequency (kHz)	Peak-Peak amplitude (mV)
18	1499	732	3188
9	1491	732	3139
5	1482	732	3143
3	1463	732	3104
0	1454	732	3090
0	1477	732	3082
-3	1431	732	3059
-3	1435	732	3064
-3	1624	586	1770
-4	1655	341	683
-4	1738	268	389
-20	3082	219	158
-21	3236	342	33
-21 aged	3686	537	1214
-21 aged	3679	537	1197
-21 aged	3679	586	1383
-21 aged	3709	634	1670

In Figure 5, we summarize the observed changes in the acoustic properties of the brine as a function of temperature.

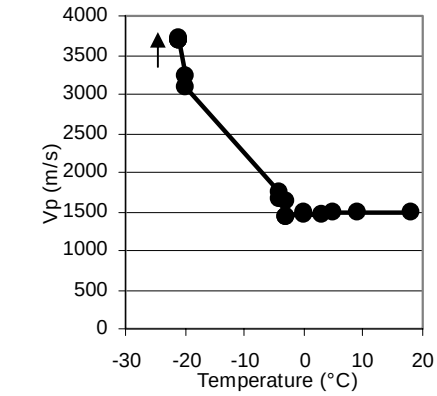

A

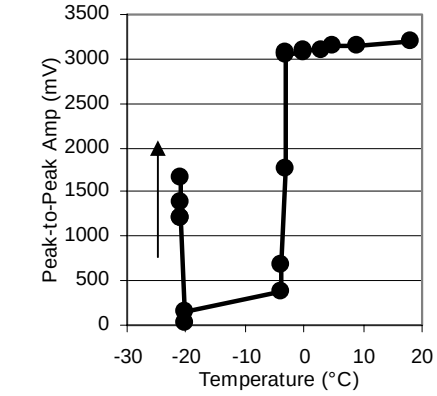

B

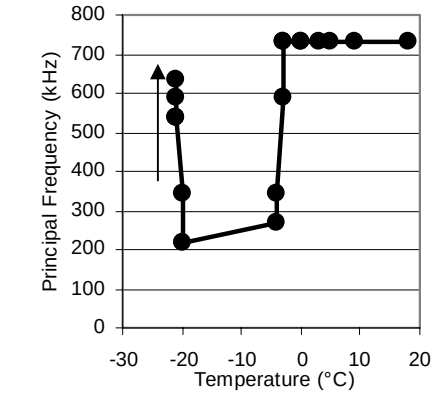

C

Figure 5. Velocity (A), peak-to-peak amplitude (B), and frequency (C) in the brine as a function of temperature. The arrow marks changes observed with increasing time as the brine matures in the freezer at a constant temperature.

Finally, in Figure 6, we show how the velocity and frequency vary with time at -21ºC as the frozen sample matures. The increase in the velocity is not large as compared to the velocity increase that occurred during freezing. However, the frequency recovers and so does the amplitude (Table 1), although not quite to their original values in liquid brine at room conditions.

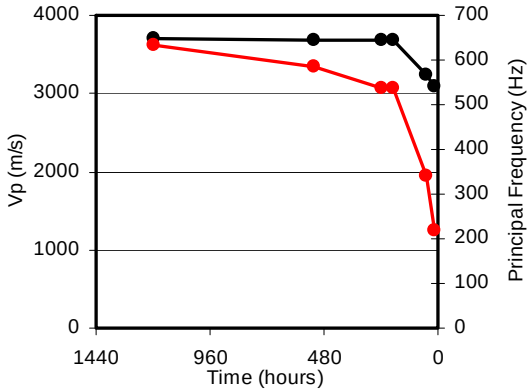

Figure 6. Velocity (black, left axis) and principal frequency (red, right axis) versus elapsed time as the frozen brine matures for about two months at -21ºC.

Conclusions

The main result from our experiment that as the brine freezes the velocity increases and so does the attenuation is somewhat unexpected. The intuition tells us that the faster the material the smaller the attenuation. However, the results presented here counter this common assumption.

At this point we avoid any speculations about the nature of the observed phenomenon – several reasons for it may exist, including artifacts of ultrasonic pulse transmission – or any generalization of these results. Also, we do not resort to complicated theory that would explain these results.

In order to confidently generalize and mathematically describe the phenomenon, more experiments have to be and will be conducted and their practical and fundamental significance established.

Acknowledgements

This work was financially supported by the Stanford Rock Physics Laboratory as well as by DOE (Award No. DE-FC26-01BC15354) and NSF. Encouragement and advice from Richard Uden of Rock Solid Images and Masami Hato of Japex are highly appreciated.

References

Guerin, G., Goldberg, D., and Meltser, A., 1999, Characterization of in situ elastic properties of gas hydrate-bearing sediments on the Blake Ridge, Journal of Geophysical Research, 104, 17781-17796.

Sakai, A., 1999, Velocity analysis of vertical seismic profile (VSP) survey at JAPEX/JNOC/GSC Mallik 2L-38 gas hydrate research well, and related problems for estimating gas hydrate concentration, in Scientific Results from JAPEX/JNOC/GSC Mallik 2L-38 gas hydrate research well, Mackenzie Delta, Northwest Territories, Canada, edited by Dallimore, S.R., Uchida, T., and Collett, T.S., Bulletin of the Geological Survey of Canada, 544, 323-340.

Wood, W.T., Holbrook, W.S., and Hoskins, H., 2000, In situ measurements of P-wave attenuation in the methane hydrate- and gas-bearing sediments of the Blake Ridge, Proceedings of Ocean Drilling Program, Scientific Results, 164, 253-264.

Guerin, G., and Goldberg, D., 2002, Sonic waveform attenuation in gas hydrate-bearing sediments from the Mallik 2L-38 research well, Mackenzie Delta, Canada, Journal of Geophysical Research, 107, 1029-1041.

Pratt, R.G., Bauer, K., and Weber, M., 2003, Crosshole waveform tomography velocity and attenuation images of arctic gas hydrate, 73rd SEG Annual Meeting in Dallas, Expanded Abstracts.

PAPER 3

Prasad, Olsen, and Fabricius: ROCK PHYSICS AND STASTICAL WELL LOG ANALYSES IN CARBONATES

Paper 1: Total of seven figures in paper

Rock Physics and Stastical Well Log Analyses in Carbonates

Manika Prasad, Department of Geophysics, Stanford University, Casper Olsen, Ida Fabricius, Environment & Resources DTU, Technical University of Denmark, Kgs. Lyngby, Denmark*

Summary

Chalks and marl reservoirs may maintain high porosity at more than two kilometers of burial depths due to overpressure and the presence of hydrocarbons. As a result, formation stability is compromised considerably and wells are is danger of being lost. Analyses of the variations in velocity, attenuation, and static compression modulus in carbonates allow us to better interpret seismic measurements in terms of subsurface petrophysical parameters and to understand the failure and damage potential. We present a study of variations in dynamic moduli in various carbonate reservoirs. Our study includes log and laboratory data from velocity, porosity, permeability, and attenuation measurements.

Introduction

Chalks and marl reservoirs may maintain high porosity at more than two kilometers of burial depths due to overpressure and the presence of hydrocarbons. As a result, formation stability is compromised considerably and wells are in danger of being lost. Analyses of the variations in porosity, clay content, and compressional velocity and modulus in carbonates allow us to better interpret seismic data in terms of subsurface petrophysical parameters and to understand the failure and damage potential. We present a study of variations in dynamic moduli in various carbonate reservoirs. Our study includes log data of velocity, porosity, vshale, and resistivity measurements.

We present analyses of well logs from the region. The analyses using rock physics models and statistical principal component analyses allow us to better understand the reservoirs and to differentiate between the different response of oil-bearing and water-bearing wells. Thus, we find that the first three principal components can explain about 80% of the data. The oil-bearing wells can be separated from the water-bearing wells by examining the first three principal components. We also show how such statistical analyses can be understood and used to make more meaningful using rock-physics models.

Location

We analyzed well logs from the chalks, limestones, and marls from the Valdemar Field located in the central Graben in the North Sea (see Figure 1). The Valdemar field in the North Sea is a low relief marly chalk structure, sealed from the overlying Chalk by calcareous shale. Six wells were used for this study. Table 1 gives a summary of the wells used in the study.

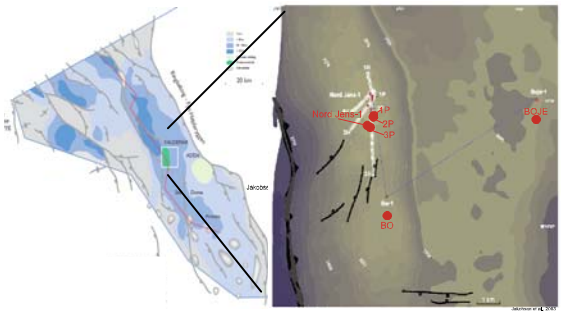

Figure 1: Location of the study area (left) and well location (right)

Table 1: Wells used in the study

Well name	Well type	Fluid type
BO	Exploration	Water
BOJE	Exploration	Water
NJENS	Exploration	Oil
VAL1P	Production	Oil
VAL2P	Production	Oil
VAL3P	Production	Oil

Raw Data from Well Logs

Figure 2 presents the well logs used in this study. We used Caliper (Cal), Gamma Ray (GR), Neutron Porosity (NPHI), LithoDensity (RHOB), Resistivity (RT), and Sonic Logs (DTP) for our analyses.

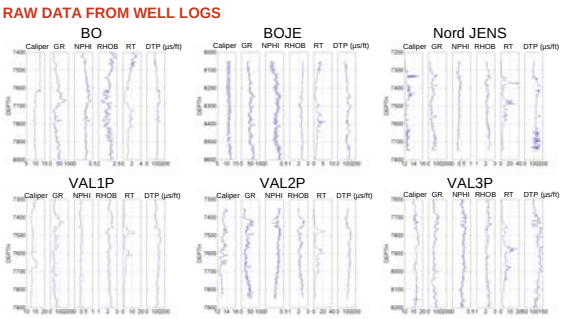

Figure 2: Raw data from the well logs

From the data presented in Figure 2, we do not observe any apparent differences between the oil and water wells. In this study, we examine the rock physics properties of the different wells. We use statistical Principal Component

Analyses to improve the rock physics models, to understand the various correlations between the different parameters, and to examine the differences between oil-bearing and water-bearing carbonate formations in the different wells.

Results

Rock Physics Relations: Figure 3 shows the rock physics relations derived for all the wells. In the plots of P-wave slowness (DTP) against porosity (NPHI), the symbols are color-coded by values of gamma ray logs (GR). Although, there is a correlation between DTP and porosity and GR, the scatter is quite large.

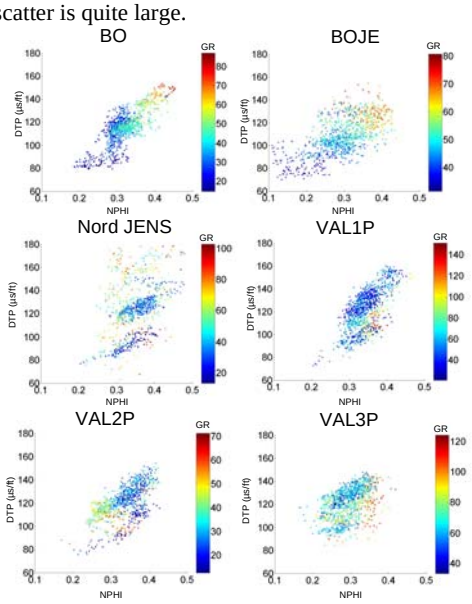

Figure 3: Porosity – DTP relations for all wells.

Principal Component Analyses: We made Principal Component (PC) analyses of all the wells using depth, gamma ray logs (GR), neutron porosity (NPHI), lithodensity (RHOB), shallow resistivity (RT), and P-wave slowness (DTP) as input parameters for our analyses. The PC analyses were made on all wells together and on each well separately. Table 2 gives the values of the first three principal components for all wells.

Table 2: First, Second, and Third PC values based on depth, GR, NPHI, PHOB, RT, and DTP in the wells used in the study.

	PC1	PC2	PC3
Depth	0.2851	0.3970	0.7423
GR	0.1513	0.7268	-0.2189
NPHI	-0.4728	0.2661	-0.3649
RHOB	0.5432	0.0435	-0.1738
RT	-0.4049	-0.2087	0.4644
DTP	-0.4618	0.4448	0.1485

From the Principal Component (PC) values in Table 1, we can distinguish between the correlations in the data set for the wells. Thus, NPHI, RHOB, DTP, and RT (saturation) play a major role in PC1. NPHI and DTP have a negative correlation with RHOB: As porosity increases, slowness also increases and density decreases.

The main contributions in PC2 are GR and DTP with some minor effects of NPHI, Depth, and RT. GR has a positive correlation with DTP. As clay content increases, slowness also increases. This observation is consistent with the laboratory data on sandstones that show a decrease in acoustic velocities with increasing clay content (Han et al., 1986; Prasad et al., 2002). The data in Table 2 suggests that there might be a depth dependence of the clay content. Also, the fact that NPHI has a large contribution but not RHOB implies a water saturation effect. Finally, the PC3 is describes by effects of mainly Depth, NPHI, and RT.

In Figures 4 and 5, we present our PC analyses of all wells together (top figures) and each well separately (bottom figures).

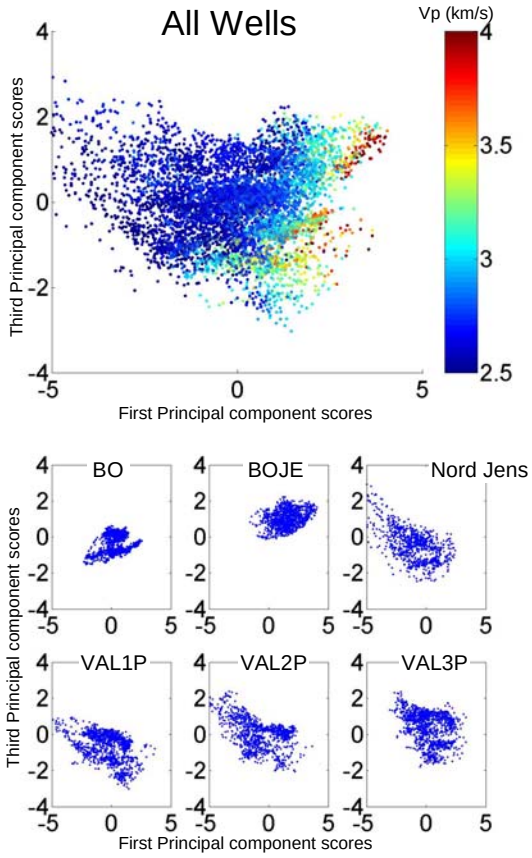

Figure 4: Relations between First and Third Principal Components for all wells (top) and each well (Bottom)

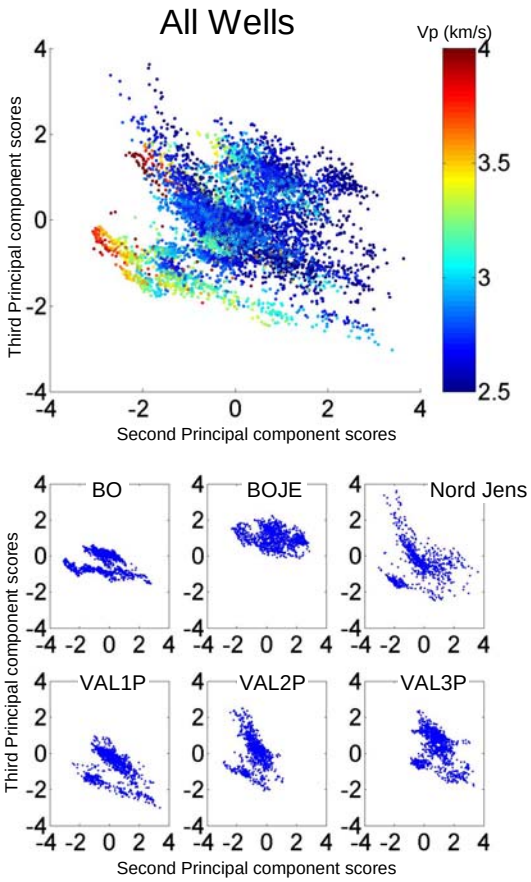

Figure 5: Relations between Second and Third Principal Components for all wells (top) and each well (Bottom)

Understanding Lithology: Figure 6 shows the results of principal component analyses on the well logs. The scatter in the 1st and 2nd principal components for NJens can be better understood by separating the trends for the water-bearing Sola Formation and the oil-bearing Tuxen Formation. In Bo and Boje wells, both formations are water-bearing.

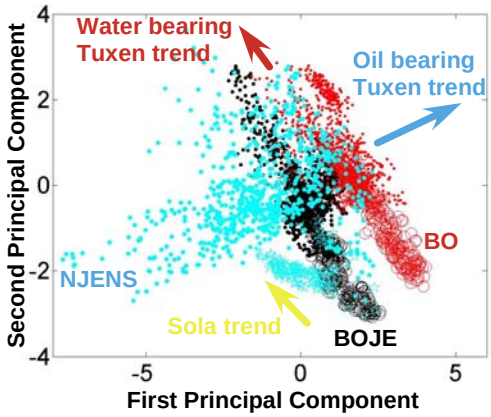

Figure 6: Crossplot of the First and Second Principal Components for three wells. Both water bearing wells, BO and BOJE show a similar trend (the Tuxen trend). The oil well (NJENS) shows a very different trend (the Sola trend).

Rock Physics Transforms for Velocity: Next, we calculated P-wave velocity for each well using the uncemented model from Dvorkin et al. (1999). The results of our calculations are shown as solid lines in Figure 7. The well log data for each well is shown as symbols color coded by clay content as calculated from the gamma ray (GR) logs. The solid lines in Figure 7 were calculated for calcite - clay mixtures from 100% calcite to a 50-50 calcite-clay mixture. We will present the variations in rock physics models that need to be considered in modeling these carbonate lithologies and compare them to other existing models to identify a best scheme to make realistic predictive models of carbonate reservoirs.

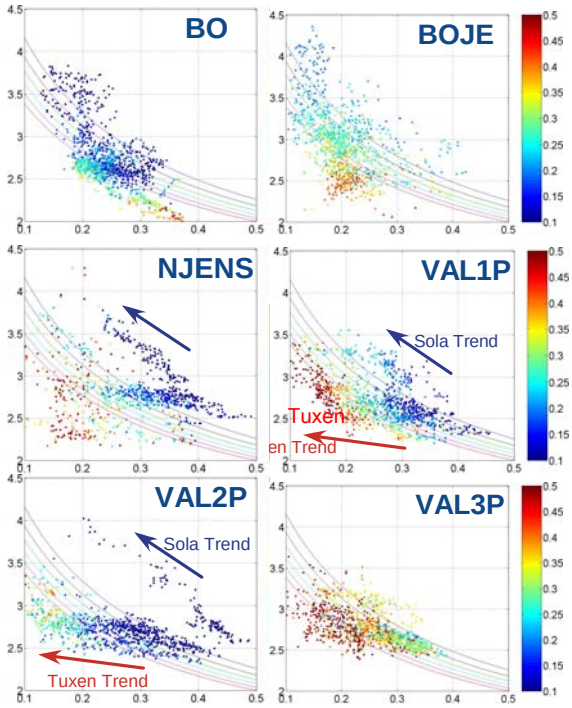

Figure 7: Relations between Second and Third Principal Components for all wells (top) and each well (Bottom)

Differentiating Fluids

To further examine the differences between the different fluids in the wells, we investigated the correlations between the PCs of each well. Table 3 shows the correlation coefficient values. The correlation coefficient patterns between oil- and water-bearing wells follow different schemes: Water-bearing wells have a negative-positive-negative sequence, whereas oil-bearing wells have a positive-negative-negative sequence.

Table 3: Correlation coefficients between PC1-PC2, PC1-PC3, and PC2-PC3 for all wells. Water-bearing wells have a negative-positive-negative sequence, whereas oil-bearing wells have a positive-negative-negative sequence.

	PC1-PC2	PC1-PC3	PC2-PC3	Fluid
BO	-0.742	0.341	-0.186	Water
BOJE	-0.821	0.325	-0.265	
NJENS	0.049	-0.659	-0.173	Oil
VAL1P	-0.050	-0.448	-0.333	
VAL2P	0.181	-0.491	-0.215	
VAL3P	-0.149	-0.324	-0.294	

Conclusions

Our rock physics and statistical analyses of well log data from the Valdemar field in North Denmark show that:

1. The correlation coefficient patterns between oil- and water-bearing wells follow different schemes: Water-bearing wells have a negative-positive-negative sequence, whereas oil-bearing wells have a positive-negative-negative sequence.
2. The scatter in the 1st and 2nd principal components for NJens can be understood by separating the trends for the water-bearing Sola Formation and the oil-bearing Tuxen Formation. In Bo and Boje wells, both formations are water-bearing.
3. Using the principal component analyses, we can make different rock physics models: the Sola can be better approximated by the cemented contact model, whereas the Vp in the Tuxen formation matches the Uncemented Sediment Model by Dvorkin et al. (1999).

References

Dvorkin, J., Prasad, M., Sakai, A., Lavoie, D., 1999, Elasticity of marine sediments: Rock Physics Modeling: GRL, v. 26, no. 12, 1781-1784.

Han, De-hua , Nur, A., and Morgan F. D., 1986. The events of porosity and clay content on wave velocities in sandstones, Geophysics, 51, 2093-2107.

Prasad, M., Reinstaedler, M., Nur, A., Arnold, W., 2002, Quantitative acoustic microscopy: Applications to petrophysical studies of reservoir rocks: Acoustical Imaging 25, Kluver Publications.

Acknowledgements

Thanks to Finn Jacobsen, Helle Christensen, Tapan Mukerji, Mark Zoback for comments. The funding and data for this work was provided by the Maersk Oil and Gas Company, the SRB project, and DOE (Award No. DE-FC26-01BC15354).

BIBLIOGRAPHY

1. Prasad, M., and Mukerji, T., Analysis of Microstructural Textures and Wave Propagation Characteristics in Shales: Expanded Abstract SEG International Exposition and Seventy-Third Annual Meeting.
2. Prasad, M., and Nur, A., Velocity and Attenuation Anisotropy in Reservoir Rocks: Expanded Abstract SEG International Exposition and Seventy-Third Annual Meeting.
3. Vega, S., Mukerji, T., Mavko, G., and Prasad, M., Stratification in loose sediments and its seismic signature: Expanded Abstract SEG International Exposition and Seventy-Third Annual Meeting.